Non-Markovian Linear Vibrational Absorption Spectroscopy for Nonharmonic Bond Potentials: A Perturbative Approach

Hélène Colinet, Florian N. Brünig, and Roland R. Netz*
Fachbereich Physik, Freie Universität Berlin, Arnimallee 14, 14195 Berlin, Germany

(Received 26 September 2024; revised 30 May 2025; accepted 25 September 2025; published 31 October 2025)

The dynamic coupling of a vibrating molecular bond to its responsive liquid environment can be described by non-Markovian friction in the framework of the generalized Langevin equation (GLE) and gives rise to line shifts as well as homogeneous and inhomogeneous spectral line broadening. By perturbation theory, we investigate how the interplay of nonharmonic bond-potential contributions and non-Markovian friction determines vibrational line shapes and positions. The accuracy of our perturbation theory is checked by simulations of the GLE. Based on bond potentials and time-dependent friction functions extracted from *ab initio* molecular dynamics simulations, our analytic theory traces the inhomogeneous line broadening of the infrared OH-stretch band of liquid water back to the coupling of non-Markovian friction to cubic and quartic bond-potential contributions.

DOI: 10.1103/btts-7ym9

Infrared (IR) spectroscopy explores molecular vibrations through infrared absorption and emission, revealing vital details about a molecule's chemical surroundings [1–6]. The positions and shapes of absorption bands offer detailed insight into molecular structure and solvation dynamics. Variances in bond length, mass, and, most distinctively, local chemical environment, produce characteristic changes of absorption peak positions and line shapes. Specifically, symmetric narrow peaks indicate homogeneous environments, while inhomogeneous environments lead to more complex broader profiles. The correlation between line position, shape, and molecular environment in IR spectroscopy enables elucidation of molecular structure, intermolecular interactions, and conformational changes, facilitating precise chemical analysis. Applications involving water [7–14] benefit from the capability of IR spectroscopy to discern subtle changes in hydrogen bonding configurations and coupling [15–19], enabling studies of hydration dynamics [20], solvation phenomena [21], and transition rates [22,23]. In the realm of protein folding [24–26], IR spectroscopy provides valuable insights into the conformational changes and structural rearrangements occurring during the folding process, contributing to our understanding of protein stability and function. However, while IR experiments offer very high precision in probing line position and shape [4], the theoretical interpretation of IR spectra remains underdeveloped. In particular, it is challenging to trace inhomogeneous line broadening mechanisms and peak shifts from their genesis due to environmental factors to the resultant changes of spectral bands. For this, one has to describe the frequency-dependent energy dissipation of a given vibrational mode within a molecule as well as into the solvent, alongside resonances between different vibrational modes and their overtones. These effects happen on multiple timescales. A very useful concept involves the non-Markovian, i.e., time-dependent, friction acting on a vibrating bond, whose significance in the context of IR spectroscopy and vibrational relaxation has been convincingly demonstrated [27–32]. Time-dependent friction arises in coarse-grained stochastic modeling of many-body dynamics and describes the dynamic coupling between reaction coordinates and their environment [22,23,31,33–41]. While quickly decaying friction contributions lead to homogeneous line broadening, friction that decays more slowly than the vibrational timescales describes slow changes in the environment and induces inhomogeneous line broadening and line shifts [31,42]. In particular, the time- (or, equivalently, frequency-) dependent friction memory strongly couples to nonharmonic potential contributions [31], motivating the development of a comprehensive analytical theory using this timescale bridging structure. Note that in our Letter, "memory" refers specifically to time-dependent friction, not to the lifetime of oscillations, which has been amply studied experimentally and theoretically [15,30], but is not considered by us. Linear IR spectroscopy experiments quantify the absorbed power of light at angular frequency $\omega = 2\pi f$, directly proportional to the imaginary component of the dielectric susceptibility $\tilde{\chi}(\omega)$. Through linear-response theory, $\tilde{\chi}(\omega)$ is linked to the autocorrelation of the total dipole moment.

*Contact author: rnetz@physik.fu-berlin.de

Published by the American Physical Society under the terms of the Creative Commons Attribution 4.0 International license. Further distribution of this work must maintain attribution to the author(s) and the published article's title, journal citation, and DOI.

This connection enables the computation of IR spectra from equilibrium simulations and theory. In this Letter, we analytically calculate the electric susceptibility by applying perturbation theory to a nonharmonic potential model with time-dependent friction memory.

The generalized Langevin equation (GLE) was introduced by Mori [43] and Zwanzig [44] in the 1960s by an exact projection of the full dynamics of a multiparticle system onto a reduced set of coordinates. All GLE parameters are uniquely determined and can be accurately extracted from simulations [22,31–33]. For the observable $x(t)$, corresponding to the bond length for vibrational spectroscopy, the GLE reads [45,46]

$$m\ddot{x}(t) = -U'[x(t)] - \int_{-\infty}^{\infty} \mathrm{d}t' \Gamma(t-t')\dot{x}(t') + F_R(t) + F_{\mathrm{ext}}(t), \tag{1}$$

where the external force (i.e., the electric field) is denoted as $F_{\mathrm{ext}}(t)$ and the friction memory kernel as $\Gamma(t-t')$. We define $\Gamma(t)$ to be single sided, i.e., $\Gamma(t) = 0$ for $t < 0$. The random force $F_R(t)$ is assumed to be Gaussian, with a mean of zero $\langle F_R(t)\rangle = 0$ and a variance that fulfills the relation $\langle F_R(t)F_R(t')\rangle = k_B T\Gamma(|t-t'|)$ [47]. The general time-independent potential $U(x)$ corresponds to the free energy profile. Note that this form of the GLE has recently been further generalized [46,48]. We define Fourier transforms as $\mathcal{F}[x(t)] = \tilde{x}(\omega) = \int_{-\infty}^{\infty} \mathrm{d}t\, e^{i\omega t}x(t)$. In the harmonic case, $U(x) = (k/2)x^2$, the response to the external force in Fourier space is linear, $\tilde{x}_0(\omega) = \tilde{\chi}_0(\omega)[\tilde{F}_R(\omega) + \tilde{F}_{\mathrm{ext}}(\omega)]$, with $\tilde{\chi}_0(\omega)$ denoting the linear response function between the applied force and the position on the harmonic level (see Supplemental Material (SM), Sect. I [49])

$$\tilde{\chi}_0(\omega) = \frac{1}{k - m\omega^2 - i\omega\tilde{\Gamma}(\omega)}. \tag{2}$$

The absorption coefficient $\omega\chi_0''(\omega)$ is proportional to the imaginary part of the linear response [52], and, in the case of constant friction $\tilde{\Gamma}(\omega) = \gamma$, reduces to the Lorentzian line shape, which is commonly used in fitting vibrational spectra [60]

$$\omega\tilde{\chi}_0''(\omega) = \frac{\gamma\omega^2}{(k - m\omega^2)^2 + \gamma^2\omega^2}. \tag{3}$$

In this case, the peak is located at the eigenfrequency of the undamped oscillator, $\omega_0 = \sqrt{(k/m)}$, has a height equal to the inverse friction $\omega_0\tilde{\chi}_0''(\omega_0) = 1/\gamma$, and a full width at half maximum (FWHM) σ that is the inverse of the inertial relaxation time $\sigma = (\gamma/m) = 1/\tau_m$, as shown in Fig. 1(a). For a nonharmonic potential $U(x) = (k/2)x^2 + (k_3/3)x^3 + (k_4/4)x^4$, the response is expanded in powers of k_3 and k_4

$$\tilde{x}(\omega) = \tilde{x}_0(\omega) + k_3\tilde{x}_1(\omega) + k_4\tilde{x}_2(\omega) + k_3^2\tilde{x}_3(\omega) + k_3k_4\tilde{x}_4(\omega) + k_4^2\tilde{x}_5(\omega) + \ldots \tag{4}$$

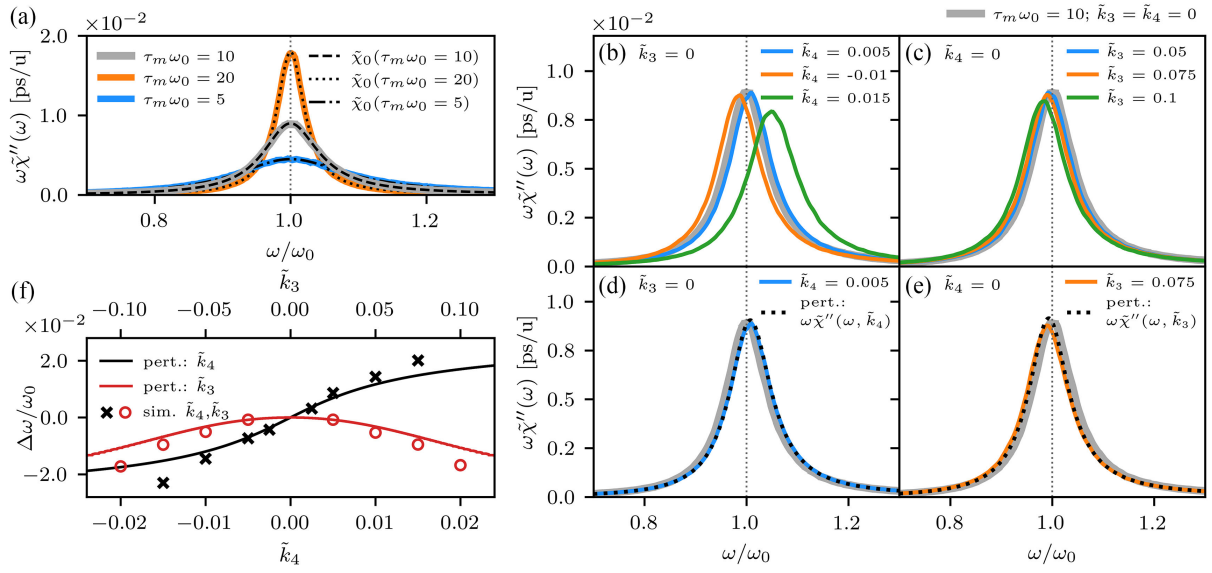


FIG. 1. Vibrational power spectra for the Markovian model with frequency-independent friction $\tilde{\Gamma}(\omega) = \gamma$. (a) Simulated absorption spectra $\omega\tilde{\chi}''(\omega)$ for different rescaled relaxation times $\tau_m\omega_0$, using a harmonic potential (thick gray, blue and orange solid lines), compared to Eq. (3) (thin black lines). (b)–(e) Comparison of the harmonic case for $\tau_m\omega_0 = 10$ (solid gray line) to nonharmonic results; (b),(c) Simulations with quartic and cubic contributions with reduced potential coefficient parameters $\tilde{k}_4 = k_4/k_BT(k/k_BT)^{-2}$ and $\tilde{k}_3 = k_3/k_BT(k/k_BT)^{-3/2}$, respectively (solid coloured lines). (d),(e) Comparison of selected simulation spectra from (b) and (c) to the perturbation prediction Eq. (5) (dotted black line). (f) Change in peak position $\Delta\omega/\omega_0$ depending on the nonharmonic coefficients: perturbation prediction Eq. (5) for the quartic (black solid line) and cubic case (red solid line), compared to simulation results for selected values of $\tilde{k}_4$ (black crosses) and $\tilde{k}_3$ (red circles). For all results we set $k = 0.25k_BT/\mathrm{pm}^2$ and $m = 1$ u.

Perturbation terms are computed by inserting the series Eq. (4) into the Fourier transformed version of the nonlinear GLE Eq. (1). The linear response $\tilde{\chi}(\omega)$, defined by the first-order expansion in $\tilde{F}_{\mathrm{ext}}(\omega)$, $\langle\tilde{x}(\omega)\rangle = \tilde{\chi}(\omega)\tilde{F}_{\mathrm{ext}}(\omega)$, accounts for nonharmonic contributions to the potential $U(x)$ and is obtained by averaging over the random force (for the comprehensive derivation, see SM, Sect. I [49]). The linear response to quadratic order in k_3, k_4 is given by

$$\tilde{\chi}(\omega) = \tilde{\chi}_0(\omega) + k_4\tilde{\chi}_{0,1}(\omega) + k_3^2\tilde{\chi}_{2,0}(\omega) + k_4^2\tilde{\chi}_{0,2}(\omega) \tag{5}$$

with the explicit kernels

$$\begin{aligned}
\tilde{\chi}_{0,1}(\omega) &= -3\frac{k_BT}{k}\tilde{\chi}_0^2(\omega),\\
\tilde{\chi}_{2,0}(\omega) &= 2\left(\frac{k_BT}{k}\tilde{\chi}_0^2(\omega)\tilde{\chi}_0(0) + 2k_BT\tilde{\chi}_0(\omega)2I_1(\omega)\right),\\
\tilde{\chi}_{0,2}(\omega) &= 9(k_BT)^2\tilde{\chi}_0^2(\omega)\left(\frac{1}{k^2}\tilde{\chi}_0(\omega) + \frac{2}{k}I_1(0) + 2I_2(\omega)\right),
\end{aligned} \tag{6}$$

where the integrals are defined as

$$I_1(\omega) = \int\frac{\mathrm{d}\omega'}{2\pi}\tilde{\chi}_0(\omega')\tilde{\chi}_0(-\omega')\tilde{\Gamma}(\omega')\tilde{\chi}_0(\omega-\omega'), \tag{7}$$

$$I_2(\omega) = \int\frac{\mathrm{d}\omega'}{2\pi}\tilde{\chi}_0(\omega')\tilde{\chi}_0(-\omega')\tilde{\Gamma}(\omega')I_1(\omega-\omega'). \tag{8}$$

Note that we neglect nuclear quantum effects.

Markovian case—We first investigate line shapes for Markovian friction, $\tilde{\Gamma}(\omega) = \gamma$. The simulation methods and extraction of the spectra are described in Sects. II and III of SM [49], respectively. In the harmonic case, the simulated spectrum reduces to the Lorentzian line shape Eq. (3), as shown in Fig. 1(a). For larger friction, the line shape flattens. In the nonharmonic case shown in Figs. 1(b) and 1(c), where we define the reduced potential coefficients $\tilde{k}_3 = k_3/k_BT(k/k_BT)^{-3/2}$ and $\tilde{k}_4 = k_4/k_BT(k/k_BT)^{-2}$, quartic potentials lead to blueshifts or redshifts depending on the sign of the potential coefficients, while cubic potentials induce redshifts only, in line with the expectation based on the effective bond stiffening or softening due to the nonharmonic contributions. These shifts are accompanied by weak line broadening (see SM, Sect. IV [49]). As shown in Figs. 1(d) and 1(e), our perturbation theory (dotted black lines) reproduces the simulated line shapes perfectly for $\tilde{k}_3 = 0.075$, $\tilde{k}_4 = 0.005$ and quantitatively predicts the line shift for not too high anharmonic potential strengths, as shown in Fig. 1(f). In SM, Sect. IV [49], we present the individual perturbation terms according to Eqs. (5) and (6).

Non-Markovian case—We first consider a friction function in the form of a single exponential, $\Gamma(t) = (\gamma/\tau^e)e^{-t/\tau^e}$, with memory time τ^e. Figure 2(a) shows how increasing τ^e leads to peak narrowing and to a blueshift that is maximal for $\tau^e\omega_0 = 1$, see the blue solid line in Fig. 2(b). The blueshift or redshift due to the nonharmonic potential contributions in Fig. 2(b) mirrors the Markovian results in Fig. 1 and is largely independent of the memory time. Typical experimental or simulated systems are characterized by multiexponential memory [34].

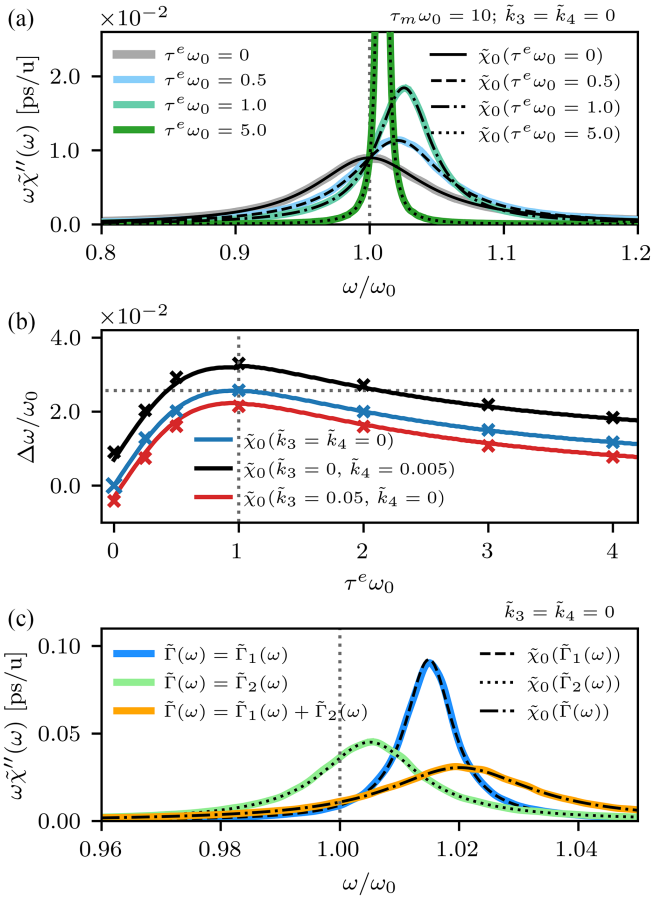


FIG. 2. Vibrational power spectra of the non-Markovian model. (a) Absorption spectra $\omega\tilde{\chi}''(\omega)$ for single-exponential kernel $\Gamma(t) = (\gamma/\tau^e)e^{-t/\tau^e}$ extracted from simulations for ascending memory time $\tau^e\omega_0$ and constant $\tau_m\omega_0 = 10$, using a harmonic potential (thick lines), compared to $\tilde{\chi}_0(\omega)$ in Eq. (2) (thin black lines). (b) Change in peak position $\Delta\omega/\omega_0$ for single-exponential memory as a function of $\tau^e\omega_0$ for a harmonic (blue) and added cubic (red) and quartic (black) potential. The prediction from perturbation theory in Eq. (5) (solid lines) is compared to simulations for $\tilde{k}_3 = 0.05$ (red crosses) and $\tilde{k}_4 = 0.005$ (black crosses). (c) Spectra for two different single-exponential kernels: $\Gamma_1(t)$ with $\tau_{m_1}\omega_0 = 10$ and $\tau^e\omega_0 = 3.0$ (larger friction and longer memory time, solid blue line) and $\Gamma_2(t)$ with $\tau_{m_2}\omega_0 = 40$ and $\tau^e\omega_0 = 0.5$ (smaller friction and shorter memory time, solid green line), compared with the biexponential kernel $\Gamma(t) = \Gamma_1(t) + \Gamma_2(t)$ (solid orange line). Simulations (colored lines) are compared with Eq. (3) (black lines). For all results we set $k = 0.25k_BT/\mathrm{pm}^2$ and $m = 1$ u.

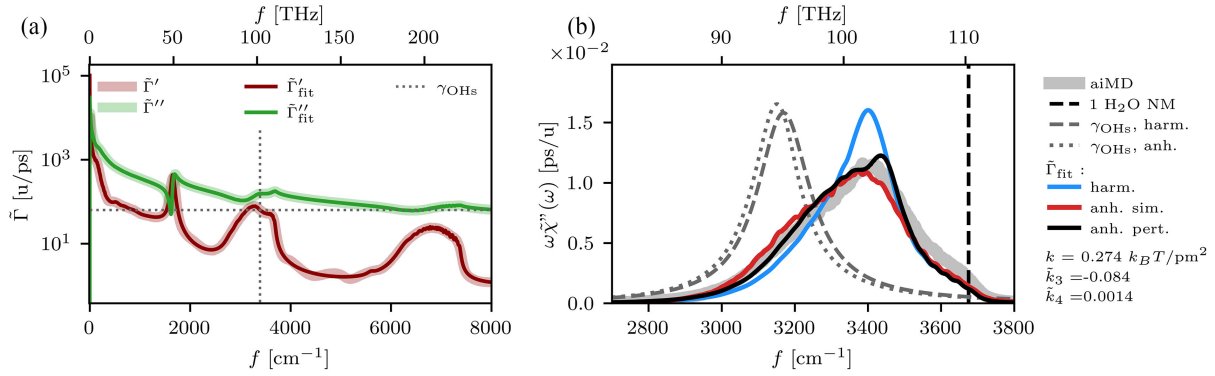


FIG. 3. Results for the symmetric stretch band $d_{\rm OHs}$ of liquid water from aiMD simulations: [31] (a) Frequency-dependent friction $\tilde{\Gamma}(\omega) = \tilde{\Gamma}'(\omega) + i\tilde{\Gamma}''(\omega)$ (thick transparent lines) with a fit $\tilde{\Gamma}_{\rm fit}(\omega)$ consisting of 10 exponential and 70 exponential-oscillating friction functions (thin solid lines). The real part is shown as red and the imaginary part as green lines. The real friction coefficient $\gamma_{OHs} = \tilde{\Gamma}(f_{\rm OHs})$ is evaluated at the symmetric stretch frequency $f_{\rm OHs} = 3390\ {\rm cm}^{-1}$. (b) The aiMD simulation vibrational power spectrum $\omega\tilde{\chi}''$ (solid gray line) is compared to models of varying complexity: the normal mode of a single water molecule at $f = 3675\ {\rm cm}^{-1}$ (vertical broken line); the harmonic Lorentzian Eq. (3) with $\gamma_{\rm OHs}$ extracted in (a) (dashed gray line) as well as the nonharmonic Markovian perturbation prediction Eq. (5) (dotted gray line); finally the non-Markovian models, each using the fitted frequency-dependent friction $\tilde{\Gamma}_{\rm fit}(\omega)$: the harmonic prediction using Eq. (2) (solid blue line); the nonharmonic Markovian embedding simulation results (solid red line), for which we use all 80 fitted functions, and the perturbation prediction Eq. (5) (solid black line).

In Fig. 2(c) we show that biexponential memory produces spectra that are blueshifted and flattened compared to single-exponential spectra. To summarize, memory and nonharmonic potential contribution give rise to spectral shifts that are largely independent from each other, the combination of short and long memory contributions, however, produces nonadditive spectral effects.

Symmetric stretch band of liquid water—We now employ previous *ab initio* MD (aiMD) results for the infrared spectrum of bulk liquid water [31] to demonstrate that our perturbation theory successfully reproduces changes in line shapes and position caused by nonharmonic potential and memory contributions of water. Brünig *et al.* [31] extracted the time-dependent friction functions and time-averaged effective bond potentials for the OH stretch and HOH bend vibrations from aiMD simulations of 256 water molecules at 300 K. By parametrizing these time-dependent friction functions (see SM Sect. V [49]), we analytically compute spectra and compare them to Markovian embedding [53–55] simulations, which provide substantial computational savings over the direct integration of the GLE. Here, we show the results for the symmetric stretch mode $d_{\rm OHs}$. A comprehensive discussion of the other vibrational modes can be found in SM, Sect. V [49].

First, the friction function $\tilde{\Gamma}(\omega) = \tilde{\Gamma}'(\omega) + i\tilde{\Gamma}''(\omega)$ from aiMD of the symmetric stretch band in Fig. 3(a) (thick transparent lines) is fitted to a combination of 10 exponential and 70 exponential-oscillating friction functions (thin solid lines, see SM Sect. V for details). Evaluating $\tilde{\Gamma}'_{\rm fit}(\omega)$ at $\omega_{\rm OHs} = 2\pi f_{\rm OHs}$ yields the friction coefficient $\gamma_{\rm OHs}$ (horizontal dotted line). The kernel models the delayed response of orthogonal intra-molecular and solvent degrees of freedom and reflects the bending mode frequency $f_{\rm HOH} = 1650\ {\rm cm}^{-1}$, the fundamental OHs symmetric stretch frequency $f_{\rm OHs} = 3390\ {\rm cm}^{-1}$, and higher harmonics, illustrating distinct vibrational pathways for energy dissipation and nonlinear coupling [56–59] (see Fig. S.11 in SM Sect. VI). In Fig. 3(b), we show the vibrational spectra of the symmetric stretch mode $d_{\rm OHs}$. From the aiMD results (thick gray line), it is apparent that liquid-water hydrogen bonding and other interactions induce a significant redshift and widening compared to the normal mode of a single H_2O at $f = 3675\ {\rm cm}^{-1}$ [31] (vertical broken line). Using the friction $\gamma_{\rm OHs}$ in Fig. 3(a) is not sufficient for reproducing the peak position or the line shape: the Lorentzian for a harmonic potential [Eq. (3), dashed gray line] and the perturbation prediction for a nonharmonic potential [Eq. (5), dotted gray line] are both too strongly redshifted and not wide enough. Using the frequency-dependent friction (for the harmonic case), the spectrum determined by Eq. (2) is shown as a blue solid line. The correct peak position is recovered—however, the peak is too sharp and too high. Now additionally taking into account nonlinear potential contributions, we compare a numerical simulation of the GLE using the extracted frequency-dependent friction (red solid line) to our perturbation prediction Eq. (2) (black solid line). The quartic potential coefficient $\tilde{k}_4 = 0.0014$ is negligibly small; the cubic perturbation, however, produces a significant reduction in peak size while maintaining the correct peak frequency. Small deviations between the analytical description and the simulation results are due to the large value of the cubic potential coefficient $\tilde{k}_3 = -0.084$ that slightly exceeds the convergence radius, as demonstrated in Fig. 1(f). The integrals determining the prefactors of the

perturbation terms, Eqs. (7) and (8), consist of a convolution between the linear response $\tilde{\chi}_0(\omega)$ and the frequency-dependent friction $\tilde{\Gamma}(\omega)$ and predominantly depend on the low-frequency part of $\tilde{\Gamma}(\omega)$ (see SM, Sect. I [49]). Thus, the long-time tail of the non-Markovian friction in conjunction with potential nonlinearities leads to inhomogeneous line broadening. Memory effects play a crucial role in determining peak position, resulting in blueshifts and alterations in line width, while additional cubic and quartic potential contributions induce redshifts or blueshifts. It transpires that the coupling of long timescale non-Markovian friction with nonharmonic potential effects is particularly significant. Note that our formalism, at its present stage, does not allow for the inclusion of nuclear quantum effects without resorting to additional approximations. Future work could account for higher-order terms in the perturbation series to enhance the accuracy of the model. By including nonlinear terms in the external force $F_{\mathrm{ext}}(t)$, our perturbative approach can also be used to predict nonlinear (i.e., multiphoton) spectra, such as measured with sum-freqency-generation [61] or 2D spectroscopy [15].

Acknowledgments—Support by the DFG via SFB1349 Project No. 1D 387284271 and by the ERC Advanced Grant No. MaMemo No. 835117 is gratefully acknowledged.

[1] P. Larkin, *Infrared and Raman Spectroscopy: Principles and Spectral Interpretation* (Elsevier, New York, 2011).
[2] J. Thompson, *Infrared Spectroscopy*, 1st ed. (Jenny Stanford Publishing, New York, 2018).
[3] H. Mantsch and D. Chapman, *Infrared Spectroscopy of Biomolecules* (Wiley-Liss, New York, 1996).
[4] D. H. Rank, Rev. Mod. Phys. **34**, 577 (1962).
[5] G. B. B. M. Sutherland, Rev. Mod. Phys. **31**, 118 (1959).
[6] H. M. Randall, Rev. Mod. Phys. **10**, 72 (1938).
[7] B. Auer and J. Skinner, J. Chem. Phys. **128**, 224511 (2008).
[8] H. J. Bakker and J. L. Skinner, Chem. Rev. **110**, 1498 (2010).
[9] L. Marco, J. Fournier, M. Thämer, W. Carpenter, and A. Tokmakoff, J. Chem. Phys. **145**, 094501 (2016).
[10] F. Perakis, L. Marco, A. Shalit, F. Tang, Z. Kann, T. Kühne, R. Torre, M. Bonn, and Y. Nagata, Chem. Rev. **116**, 7590 (2016).
[11] L. Marco, W. Carpenter, H. Liu, R. Biswas, J. Bowman, and A. Tokmakoff, J. Phys. Chem. Lett. **7**, 1769 (2016).
[12] J. Stenger, D. Madsen, P. Hamm, E. T. J. Nibbering, and T. Elsaesser, Phys. Rev. Lett. **87**, 027401 (2001).
[13] M. Heyden, J. Sun, S. Funkner, G. Mathias, H. Forbert, M. Havenith, and D. Marx, Proc. Natl. Acad. Sci. U.S.A. **107**, 12068 (2010).
[14] S. Carlson, F. Brünig, P. Loche, D. Bonthuis, and R. Netz, J. Phys. Chem. A **124**, 5599 (2020).
[15] M. Cowan, B. Bruner, N. Huse, J. Dwyer, B. Chugh, E. Nibbering, T. Elsaesser, and R. Miller, Nature (London) **434**, 199 (2005).
[16] S. Woutersen, U. Emmerichs, and H. Bakker, Science **278**, 658 (1997).
[17] S. Woutersen and H. Bakker, Nature (London) **402**, 507 (1999).
[18] T. Elsaesser, Acc. Chem. Res. **42**, 1220 (2009).
[19] M. Sovago, R. Campen, G. Wurpel, M. Müller, H. Bakker, and M. Bonn, Phys. Rev. Lett. **100**, 173901 (2008).
[20] D. Laage, T. Elsaesser, and J. Hynes, Chem. Rev. **117**, 10694 (2017).
[21] F. Dahms, R. Costard, E. Pines, B. Fingerhut, E. Nibbering, and T. Elsaesser, Angew. Chem. **55**, 10600 (2016).
[22] J. Daldrop, J. Kappler, F. Brünig, and R. Netz, Proc. Natl. Acad. Sci. U.S.A. **115**, 201722327 (2018).
[23] B. J. Berne, M. Borkovec, and J. E. Straub, J. Phys. Chem. **92**, 3711 (1988).
[24] M.-C. Bellissent-Funel, A. Hassanali, M. Havenith, R. Henchman, P. Pohl, F. Sterpone, D. van der Spoel, Y. Xu, and A. Garcia, Chem. Rev. **116**, 7673 (2016).
[25] A. L. Serrano, M. M. Waegele, and F. Gai, Protein Sci. **21**, 157 (2012).
[26] F. Heinz and N. Dieter, *Protein Folding and Misfolding Shining Light by Infrared Spectroscopy* (Springer, New York, 2011).
[27] H. Metiu, D. W. Oxtoby, and K. F. Freed, Phys. Rev. A **15**, 361 (1977).
[28] T. Joutsuka and K. Ando, J. Chem. Phys. **134**, 204511 (2011).
[29] R. M. Whitnell, K. R. Wilson, and J. T. Hynes, J. Chem. Phys. **96**, 5354 (1992).
[30] M. Tuckerman and B. J. Berne, J. Chem. Phys. **98**, 7301 (1993).
[31] F. N. Brünig, O. Geburtig, A. von Canal, J. Kappler, and R. R. Netz, J. Phys. Chem. B **126**, 1579 (2022).
[32] J. E. Straub, M. Borkovec, and B. J. Berne, J. Phys. Chem. **91**, 4995 (1987).
[33] B. A. Dalton, A. Klimek, H. Kiefer, F. N. Brünig, H. Colinet, L. Tepper, A. Abbasi, and R. R. Netz, Annu. Rev. Phys. Chem. **76**, 431 (2025).
[34] G. Jung, M. Hanke, and F. Schmid, Soft Matter **14**, 9368 (2018).
[35] O. Lange and H. Grubmüller, J. Chem. Phys. **124**, 214903 (2006).
[36] I. Horenko, C. Hartmann, C. Schütte, and F. Noé, Phys. Rev. E **76**, 016706 (2007).
[37] E. Darve, J. Solomon, and A. Kira, Proc. Natl. Acad. Sci. U.S.A. **106**, 10884 (2009).
[38] D. Lesnicki, R. Vuilleumier, A. Carof, and B. Rotenberg, Phys. Rev. Lett. **116** (2016).
[39] G. Deichmann and N. van der Vegt, J. Chem. Phys. **149**, 244114 (2018).
[40] H. Meyer, T. Voigtmann, and T. Schilling, J. Chem. Phys. **150**, 174118 (2019).
[41] B. Dalton, C. Ayaz, H. Kiefer, A. Klimek, L. Tepper, and R. Netz, Proc. Natl. Acad. Sci. U.S.A. **120**, 31 (2023).
[42] D. W. Oxtoby, D. Levesque, and J. J. Weis, J. Chem. Phys. **68**, 5528 (1978).
[43] H. Mori, Prog. Theor. Phys. **33**, 423 (1965).
[44] R. Zwanzig, Phys. Rev. **124**, 983 (1961).
[45] C. Ayaz, L. Tepper, and R. R. Netz, Turk. J. Phys. **46**, 194 (2022).
[46] H. Vroylandt, Europhys. Lett. **140**, 62003 (2022).

[47] R. Kubo, J. Phys. Soc. Jpn. **12**, 570 (1957).
[48] C. Ayaz, L. Scalfi, B. A. Dalton, and R. R. Netz, Phys. Rev. E **105**, 054138 (2022).
[49] See Supplemental Material at http://link.aps.org/supplemental/10.1103/btts-7ym9 for derivations of all equations in the main text, as well as details of the methods used to simulate the trajectories and extract the infrared spectra. We provide a comprehensive overview of the effects of nonharmonic perturbations for the Markovian case, along with the results for all modes of liquid water, where we show the fitted potentials, memory kernels, and infrared spectra. The Supplemental Material includes Refs. [7,14,15,31,50–59].
[50] B. Leimkuhler and C. Matthews, *Molecular Dynamics: With Deterministic and Stochastic Numerical Methods* (Springer, New York, 2015).
[51] N. Wiener, Acta Math. **55**, 117 (1930).
[52] R. Kubo, Rep. Prog. Phys. **29**, 255 (1966).
[53] H. Risken and T. Frank, *The Fokker-Planck Equation: Methods of Solution and Applications*, Springer Series in Synergetics (Springer Science & Business Media, Berlin, 1996), p. 472.
[54] P. Siegle, I. Goychuk, P. Talkner, and P. Hänggi, Phys. Rev. E **81**, 011136 (2010).
[55] A. O. Caldeira and A. J. Leggett, Physica (Amsterdam) **121A**, 587 (1983).
[56] A. A. Kananenka and J. L. Skinner, J. Chem. Phys. **148**, 244107 (2018).
[57] C.-C. Yu, K.-Y. Chiang, M. Okuno, T. Seki, T. Ohto, X. Yu, V. Korepanov, H.-o. Hamaguchi, M. Bonn, J. Hunger, and Y. Nagata, Nat. Commun. **11**, 5977 (2020).
[58] W. Amir, G. Gallot, and F. Hache, J. Chem. Phys. **121**, 7908 (2004).
[59] P. K. Verma, A. Kundu, M. S. Puretz, C. Dhoonmoon, O. S. Chegwidden, C. H. Londergan, and M. Cho, J. Phys. Chem. B **122**, 2587 (2018).
[60] R. Meier, Vib. Spectrosc. **39**, 266 (2005).
[61] A. P. Fellows, Díaz Duque, V. Balos, L. Lehmann, R. R. Netz, M. Wolf, and M. Thämer, Langmuir **40**, 18760 (2024).